

Magnetolectric Response of Antiferromagnetic CrI₃ Bilayers

Chao Lei,^{*,†,||} Bheema L. Chittari,^{‡,||} Kentaro Nomura,[§] Nepal Banerjee,^{¶,⊥} Jeil Jung,^{*,¶,⊥} and Allan H. MacDonald[†]

[†]*Department of Physics, The University of Texas at Austin, Austin, Texas 78712, USA*

[‡]*Department of Physical Sciences, Indian Institute of Science Education and Research
Kolkata, Mohanpur 741246, West Bengal, India*

[¶]*Department of Physics, University of Seoul, Seoul 02504, Korea*

[§]*Institute for Materials Research, Tohoku University, Sendai Aoba-ku 980-8577, Japan*

^{||}*Contributed equally to this work*

[⊥]*Department of Smart Cities, University of Seoul, Seoul 02504, Korea*

E-mail: leichao.ph@gmail.com; jeiljung@uos.ac.kr

Abstract

We predict that layer antiferromagnetic bilayers formed from van der Waals (vdW) materials with weak inter-layer versus intra-layer exchange coupling have strong magnetolectric response that can be detected in dual gated devices where internal displacement fields and carrier densities can be varied independently. We illustrate this strong temperature dependent magnetolectric response in bilayer CrI₃ at charge neutrality by calculating the gate voltage dependent total magnetization through Monte Carlo simulations and mean-field solutions of the anisotropic Heisenberg model informed from density functional theory and experimental data, and present a simple model for electrical control of magnetism by electrostatic doping.

Keywords

CrI₃, Magnetoelectric Effect, van der Waals Material, Antiferromagnetic Bilayer, 2D magnets

Introduction

Spintronics studies the interplay between electrical and magnetic properties of materials and underlies an important technology that was based so far mostly on the properties¹⁻⁴ of ferromagnetic metals. There has long been interest in expanding spintronics to semiconductors,⁵ which tend to have properties that are more subject to electrical control,⁶ and usually have antiferromagnetic order. Antiferromagnets do have some potential advantages for spintronics, which have attracted attention recently.⁷⁻⁹ These advantages include insensitivity to magnetic fields, absence of stray fields, the possibility of terahertz manipulation for ultrafast switching, multiple stable domain configurations. Here, we consider the new class of two-dimensional van der Waals magnetic materials that have been fabricated for the first time relatively recently,^{10,11} for which tunneling magnetoresistance,¹²⁻¹⁵ electrical control of magnetic configurations by doping,¹⁶⁻¹⁸ and pressure-induced interlayer magnetic transition¹⁹ have already been demonstrated in CrI₃ bilayers.

Surprisingly, CrI₃ bilayers have antiferromagnetic interlayer interactions^{10,16-18} even though bulk CrI₃ is ferromagnetic. It has thus been widely studied to understand the magnetism of CrI₃ bilayers.²⁰⁻³² Since the bilayers are coupled via van der Waals (vdW) forces, the interlayer magnetic exchange interactions are also weak, and it was shown that the interlayer magnetic exchange can be tuned from antiferromagnetic to ferromagnetic just by electrostatic doping.¹⁶⁻¹⁸ Electric fields in van der Waals bilayers also alter the magnon dispersion,³³ opening a gap between bands associated with the two spins per unit cell in the two-dimensional honeycomb lattices and opening the possibility of topological magnon bands when the electric field breaks the inversion symmetry and generates Dzyaloshinskii-Moriya interactions.³⁴⁻³⁶ Even though applications await further development, still in progress,³⁷⁻⁴⁰

of well-controlled magnetic van der Waals bilayers that order at room temperature, it is not premature to contemplate the particular advantages of this class of antiferromagnetic semiconductors.

In this paper, we address the possibilities for electrical control of magnetization in CrI_3 that exemplifies a van der Waals (vdW) semiconductor bilayer with antiferromagnetic interlayer interactions. We predict by means of Monte Carlo simulations and mean-field calculations that antiferromagnetic vdW bilayers at charge neutrality will generally have strong magnetoelectric response when the interlayer antiferromagnetic exchange coupling is weaker than intralayer ferromagnetic exchange coupling. We also present a simple model for electrical control of magnetism by electrostatic doping, which has been observed experimentally.¹⁶⁻¹⁸ These effects can be detected in both single-gate devices where we can simultaneously vary the electric fields and carrier densities, and also in dual-gate geometries where they can be varied independently. Our theory presented for CrI_3 should find promising applications in other van der Waals antiferromagnetic bilayers like V-doped WSe_2 and CrTe_2 ^{39,40} where magnetic ordering at room temperature is expected. A schematic illustration in Fig. 1 shows how the magnetoelectric response can be detected by measuring the gate voltage dependence of Faraday/Kerr rotation, anomalous Hall conductivity, or bulk magnetization.

Theoretical Model for CrI_3 Bilayers

The Heisenberg model for the Cr-ion spin network contains Heisenberg exchange interactions and magnetic anisotropy. The origin of magnetic anisotropy has been widely studied and is still under debate.⁴¹⁻⁵¹ It is still not settled whether on-site^{36,49} or exchange anisotropy⁴⁵ dominates in CrI_3 . However, as we show below, magnetic anisotropy does not play an important role in the magneto-electric response properties, provided it is sufficiently strong to avoid a strong reduction in critical temperature. We can therefore employ a Heisenberg

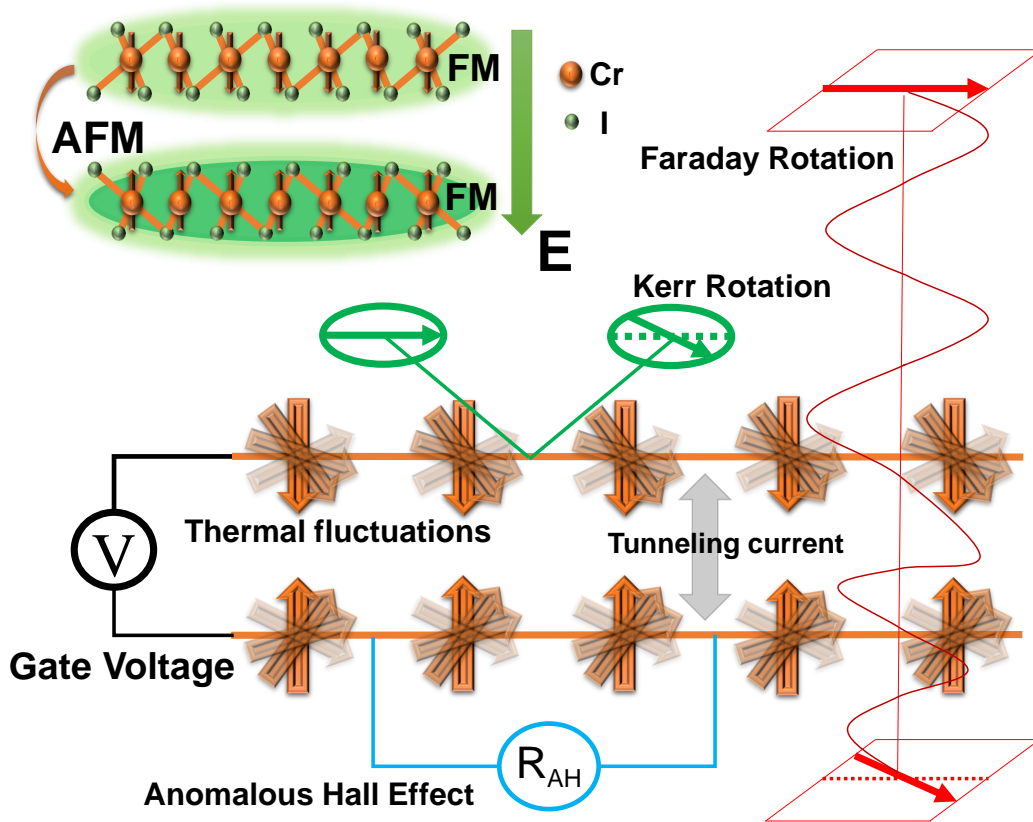


Figure 1: Schematic of magnetolectric response in bilayer CrI_3 where perpendicular gate electric fields polarize the bilayers, making exchange interactions layer dependent. At finite temperature, this leads to non-zero bulk magnetization, Faraday/Kerr rotation, and anomalous Hall conductivity.

model with on-site magnetic anisotropy without any loss of generality:

$$\mathcal{H} = -\frac{1}{2} \sum_{i, \mathbf{R}, \mathbf{R}'} J_i(\mathbf{R} - \mathbf{R}') \mathbf{S}_{i\mathbf{R}} \cdot \mathbf{S}_{i\mathbf{R}'} - \frac{1}{2} \sum_{\substack{i \neq j \\ \mathbf{R}, \mathbf{R}'}} J_v(\mathbf{R} - \mathbf{R}') \mathbf{S}_{i\mathbf{R}} \cdot \mathbf{S}_{j\mathbf{R}'} - D \sum_{i, \mathbf{R}} (S_{i\mathbf{R}}^z)^2, \quad (1)$$

where i or j are t, b labels for top/bottom layer, $J_i(\mathbf{R} - \mathbf{R}')$ is the intralayer exchange coupling and $J_v(\mathbf{R} - \mathbf{R}')$ the interlayer coupling, \mathbf{R} is the in-plane Cr ion position, \mathbf{S} is the spin operator, D is the on-site magnetic anisotropic energy. To obtain the parameters of the Heisenberg model for bilayer CrI_3 , we have compared the total energies of different spin configurations using plane wave density-functional-theory as implemented in the Vienna Ab initio simulation package(VASP)⁵² and Quantum Espresso(QE)⁵³ applied to bilayer CrI_3 , using semi-local PBE-GGA⁵⁴ with the vdW-D2 correction proposed by Grimme.⁵⁵ Both implementations show overall qualitative agreement while minor quantitative differences can exist. The equilibrium interlayer distances in van der Waals layered materials results from a delicate balance of shorter ranged chemical bonds and longer ranged Coulomb correlations which cannot be systematically captured within commonly used local or semi-local density functionals.⁵⁶ On the other hand, the intralayer electronic structures can rely on the DFT calculations because of the dominantly covalent or ionic character of the bonds. We therefore use DFT to evaluate the electric-field dependence of intralayer exchange coupling parameters, while relying on information from experiment for the interlayer exchange interactions obtained from the layer AFM-FM crossover induced by a magnetic field. The electric field is applied in VASP^{57,58} by inserting a dipole sheet in the middle of vacuum. Further discussions on the technical details of these calculations can be found in the supporting information.⁵⁹

The anisotropy energy for bilayer CrI_3 is $660 \mu\text{eV}/\text{Cr}$ according to VASP, and is $730 \mu\text{eV}/\text{Cr}$ atom according to QE. These values are smaller than the corresponding monolayer values ($D = 960 \mu\text{eV}/\text{Cr}$ in QE), and similar to the bulk value $690 \mu\text{eV}/\text{Cr}$ ⁶⁰ reported in the literature. Magnetic anisotropy plays a critical role in limiting the thermal fluctuations that lower the monolayer and bilayer critical temperatures relative to their mean-field values.

The increase of T_c with Δ estimated from Monte Carlo simulations is illustrated in Fig. S13, ⁵⁹ and is in agreement with results reported in. ⁵¹ Based on DFT calculations, the magnon energies in bilayer CrI_3 are in the range below 15 meV, and the magnon gap is around 1 meV. ⁵⁹ The exchange interaction part of the spin Hamiltonian in Eq. (1) can be expressed in momentum-space by using the Fourier transform $\mathbf{S}_{i\mathbf{R}} = 1/\sqrt{N} \sum_{\mathbf{k}} e^{i\mathbf{k}\cdot\mathbf{R}} \mathbf{S}_i(\mathbf{k})$ resulting in

$$\mathcal{H}(\mathbf{k}) = -\frac{1}{2} \sum_{i,\mathbf{k}} J_i(\mathbf{k}) \mathbf{S}_i(-\mathbf{k}) \cdot \mathbf{S}_i(\mathbf{k}) - \frac{1}{2} \sum_{\substack{i \neq j \\ \mathbf{k}}} J_v(\mathbf{k}) \mathbf{S}_i(\mathbf{k}) \cdot \mathbf{S}_j(\mathbf{k}), \quad (2)$$

where $i = t/b$ are top/bottom layer labels, $\mathbf{S}_i(\mathbf{k})$ is the appropriately normalized Fourier transform of the dimensionless (without \hbar) spin operators in layer i , and

$$J_i(\mathbf{k}) = \sum_{\mathbf{L}} \exp(-i\mathbf{k} \cdot \mathbf{L}) J_i(\mathbf{L}) \quad (3)$$

is a Fourier sum of exchange interactions between spins localized at the origin in layer i and at lattice site $\mathbf{L} \equiv \mathbf{R} - \mathbf{R}'$. The intralayer exchange constants extracted from ground state energy calculations for different metastable magnetic configurations are summarized in the supporting information. ⁵⁹

The overall weakness of interlayer magnetic interaction in CrI_3 bilayers can be expected from the relative weakness of the van der Waals interlayer coupling with respect to the intralayer bonds. Bulk CrI_3 is a layered semiconductor with a low-temperature $R\bar{3}$ rhombohedral structure ⁶¹⁻⁶⁴ illustrated in the supporting information ⁵⁹ and a high-temperature $C2/m$ monoclinic structure. We performed calculations using both LDA and LDA+U DFT approximations for both $R\bar{3}$ and $C2/m$ stacking arrangements, with and without spin-orbit coupling. Within LDA the predicted interlayer magnetic interactions are most often ferromagnetic and much stronger than experimental estimates, and we find that the monoclinic $C2/m$ structure is ferromagnetic at equilibrium interlayer distance becoming antiferromagnetic only at larger values of interlayer separation. The change in sign as d varies is expected, since direct ferromagnetic exchange interactions are expected to decline more rapidly with

d than antiferromagnetic superexchange interactions, and additional DFT results are summarized in Fig. S4 and S5⁵⁹). Note that the antiferromagnetic and ferromagnetic states reach their minimum energies at different layer separations⁵⁹ and that the vdW gaps of the encapsulated bilayers studied experimentally^{16–18} are likely smaller than those of the isolated bilayers we have studied theoretically. It follows that the field-driven antiferromagnetic to ferromagnetic transition should be accompanied by a change in the separation between layers, and that the critical field of the transition should be pressure-dependent and altered by encapsulation.

This landscape of DFT results, although not definitively predictive for interlayer exchange, establish that the interlayer magnetic interaction in CrI₃ bilayers is weak and sensitive to layer separation⁵⁹ and stacking arrangement.^{20–23,59} Below we view the interlayer magnetic interaction parameter as a quantity that is presently most reliably estimated from experiments. However, as already mentioned, the DFT calculations do reliably predict important details of the intralayer magnetic interactions $J_{t/b}$ that are related to the covalent intralayer bonding network.

Magnetolectric Response

The strength of the interlayer exchange constant $\tilde{J}_v \equiv J_v S^2$ (with $J_v \equiv \sum_{\mathbf{L}} J_v(\mathbf{L})$) can be reliably extracted from the magnetic field $B_c \approx 0.65T^{10}$ needed to drive the antiferromagnetic bilayer to a ferromagnetic state. This consideration implies that $\tilde{J}_v = 2g\mu_B S B_c \approx -0.23 \text{ meV}$ with $S = 3/2$. The interlayer exchange constant is nearly two orders of magnitude smaller than the bilayer’s ferromagnetic intralayer magnetic interaction parameter, which is denoted by $\tilde{J}_{t/b} \equiv J_{t/b} S^2$, with $J_{t/b} \equiv \sum_{\mathbf{L}} J_{t/b}(\mathbf{L})$ for top and bottom layers. In the absence of electric fields we estimate that $\tilde{J}_0 = \tilde{J}_t = \tilde{J}_b \approx 14.6 \text{ meV}$ according to DFT calculations.

To establish that weak interlayer coupling implies strong magneto-electric response, we first apply the mean-field theory to the intrinsic case where the local spin moments are the

only low-energy degree of freedom. In mean-field theory the temperature dependent moment per site depends only on the exchange coupling at $\mathbf{k} = 0$:

$$\begin{aligned}\langle \mathbf{S} \rangle_{t/b} &= \pm \hat{z} S s_{t/b} = \pm \hat{z} S B_S(\beta h_{t/b}) \\ h_{t/b} &= \left(\tilde{J}_{t/b} + H \right) s_{t/b} - |\tilde{J}_v| s_{b/t}.\end{aligned}\tag{4}$$

where the z-axis projected magnetization $s_{t/b}$ at top or bottom layer sites can assume values between -1 to 1 . The \pm signs are associated to top or bottom (t/b) layers respectively, the Hamiltonian $h_{t/b}$ includes both intra and interlayer exchange coupling. The intralayer exchange coupling term $\tilde{J}_{t/b} = \tilde{J}_0 \pm \lambda \mathcal{E}$ respectively for t and b layers includes an electric field \mathcal{E} dependent term proportional to the response coefficient λ , where \tilde{J}_0 denotes the intralayer exchange coupling in the absence of an electric field. The magnetic field H is here given in units of \tilde{J}_0 in the Zeeman term, the $\beta = 1/k_B T$ is the inverse temperature, the intralayer effective exchange coupling $\tilde{J}_{t/b} \equiv S^2 J_{t/b}(\mathbf{k} = 0) = S^2 \sum_{\mathbf{L}} J_{t/b}(\mathbf{L})$ includes all distant neighbor exchange coupling, and the interlayer $\tilde{J}_v \equiv S^2 J_v$. Both terms use $S = 3/2$ as defined above. $B_S(x)$ is the Brillouin function, and we assume that the magnetization $s_{t/b}$ points in the \hat{z} direction. In the absence of an electric field, $J_t(\mathbf{L}) = J_b(\mathbf{L})$ due to inversion symmetry in CrI_3 bilayers. $\tilde{J}_{t/b} > 0$ favors ferromagnetic alignment of spins within each layer, and $\tilde{J}_v < 0$, favors antiferromagnetic coupling between layers.

The intralayer magnetic exchange interaction from DFT calculations $\tilde{J}_{t/b} \approx 14.6$ meV corresponds to a mean-field critical temperature $T_{MF} \sim 94\text{K}$. This size of exchange interaction is in reasonable agreement with experiment since it would imply a ratio of the critical temperature to its mean-field value ~ 0.50 , slightly smaller than the ideal two-dimensional Ising model value $T_c/T_{MF} \sim 0.56$. The Monte Carlo Curie temperature we obtain for monolayers is 30 K, and the Néel temperature for bilayers is 31 K when we use the experimental antiferromagnetic interlayer coupling $\tilde{J}_v \approx -0.23$ meV. We observe that although T_c is mainly governed by intralayer exchange parameters, the interlayer coupling can help

suppress thermal fluctuations and increase T_c . (See Figs. S14-S16⁵⁹).

The magnetoelectric coupling we focus on results from mirror-symmetry breaking by a gate tunable electric field \mathcal{E} . Since $\tilde{J}_t + \tilde{J}_b$ and \tilde{J}_v must be even functions of \mathcal{E} , we can describe linear magneto-electric response by letting $\tilde{J}_{t/b} = \tilde{J}_0 \pm \lambda\mathcal{E}$ as defined earlier. It follows that the linear response to \mathcal{E} of the total spin per unit cell, where $f = S(s_t - s_b)$ uses the local moments $s_t(s_b)$,⁵⁹

$$\alpha \equiv \frac{df}{d\mathcal{E}} = \lambda\chi_F, \quad (5)$$

where χ_F is the magnetic susceptibility and

$$\chi_F \equiv \frac{df}{dH} = 2Ss_{AF} \frac{\beta B'_S(\beta h_0)}{1 - \beta(\tilde{J}_0 - |\tilde{J}_v|)B'_S(\beta h_0)}, \quad (6)$$

where $B'_S(x)$ is the derivative of $B_S(x)$, $s_{AF} = (s_t + s_b)/2$ is the average local moment of the unit cell in the $\mathcal{E} = 0$ antiferromagnetic bilayer states and becomes 1 and 0 respectively in the layer antiferromagnetic and the layer ferromagnetic configurations in virtue of the layer dependent sign definition in Eq. (4), see the supporting information.⁵⁹ The h_0 corresponds to $h_{t/b}$ with zero electric and magnetic fields. Since $|\tilde{J}_v|$ is always very small compared to \tilde{J}_0 in antiferromagnetic vdW bilayers, $\tilde{J}_0 - |\tilde{J}_v| \approx \tilde{J}_0 + |\tilde{J}_v|$. Note that $\beta(\tilde{J}_0 + |\tilde{J}_v|)B'_S(\beta h_0) = 1$ at the antiferromagnetic critical temperature. The critical divergence in χ that would occur at the transition temperature if the system was ferromagnetic is therefore only weakly truncated in the antiferromagnetic state.⁵⁹ For $T_N/T - 1 > |\tilde{J}_v|/\tilde{J}_0$ the mean-field magnetoelectric response grows like $(T_N - T)^{-1/2}$.

Fig. 2 compares the bilayer magnetoelectric response calculated using this mean-field-theory with the results of classical Monte Carlo simulations $\alpha = \langle S_z \partial \mathcal{H} / \partial \mathcal{E} \rangle / (Nk_B T)$ where \mathcal{H} is the classical spin-Hamiltonian, S_z is proportional to the total magnetization and N is the number of lattice sites per layer. See the supporting information for further details of the MC calculation. From the $\tilde{J}_0 \approx 14.6$ meV DFT results for intralayer exchange interaction and the $\tilde{J}_v \approx -0.23$ meV experimental results for interlayer exchange interaction, we have

$J_v/J_0 \approx -0.016$. Due to the sensitive dependence of interlayer exchange interaction on both interlayer distance and stacking,⁵⁹ we calculated the magnetoelectric response for various values of J_v/J_0 as shown in Fig. 2. As we discuss above, the Monte Carlo results are strongly sensitive to magnetic anisotropy which must be present to endow the mean-field calculations with qualitative validity. In antiferromagnetic bilayers with the strength of uniaxial anisotropy present in CrI_3 , the mean-field predictions are largely validated by Monte Carlo. The magnetoelectric response is largest close to but below the antiferromagnetic transition temperature.

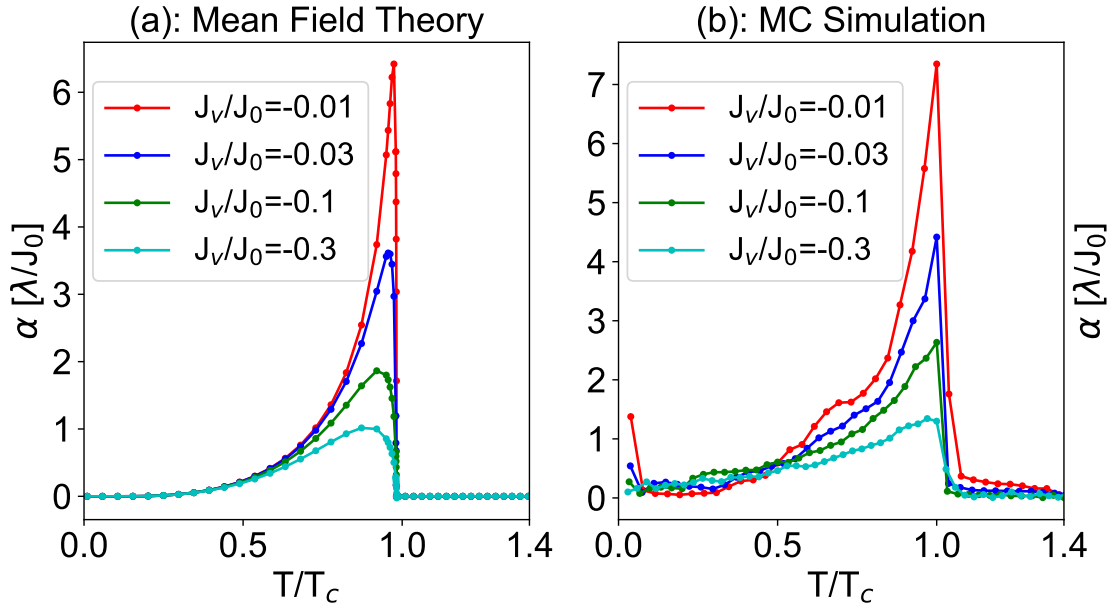


Figure 2: Magnetoelectric response of antiferromagnetic bilayers in units of λ/J_0 calculated using (a) mean-field theory and (b) numerical Monte-Carlo (MC) simulation. The MC simulation was performed using the exchange and magnetic anisotropy of CrI_3 , except that interlayer exchange was scaled to match the range of values considered in the mean-field calculations. J_0 and λ parameters are defined in Eqs. (3), (7) and respectively characterize intralayer exchange and its sensitivity to external electric fields. Using DFT estimates for the values of λ and J_F in CrI_3 , we find that the ratio of the induced magnetization per volume to the applied electric field is $\sim 10^{-4}$ times the quantity plotted in this figure. The MC magneto-electric response $\alpha = \langle S_z \partial \mathcal{H} / \partial \mathcal{E} \rangle / (N k_B T)$ was calculated from the spin correlation function where \mathcal{H} is the classical spin-Hamiltonian, S_z is proportional to the total magnetization and N is the number of lattice sites per layer.

In the absence of carriers we find from DFT calculations⁵⁹ that in CrI_3 the coupling

constant λ defined in Eq. (5) has the value

$$|\lambda| = \frac{1}{2} \frac{d(\tilde{J}_t - \tilde{J}_b)}{d\mathcal{E}} \approx 0.12 \text{ meV/V nm}^{-1}. \quad (7)$$

The sign of λ is such that the layer with the lower electric potential and higher charge density has stronger exchange interactions. Strong gate electric fields $\mathcal{E} \sim 1 \text{ Vnm}^{-1}$ yield intralayer magnetic interactions that are $\sim 2\%$ higher in the high-density layer than in the low-density layer. This relatively small variation in the intralayer exchange coupling parameters can still slightly increase the Curie temperatures (T_c) estimated by mean-field and Monte Carlo calculations.⁵⁹ In the presence of electric field, antisymmetric (Dzyaloshinskii-Moriya exchange interactions (DMI) are allowed by the breaking of inversion symmetry.³⁶ The DMI increases linearly to $\sim 0.4 \text{ meV}$ for an electric field of 1 V/nm , and thus is smaller than $\sim 0.04 \text{ meV}$ in typical experimental electric fields up to 0.1 V/nm . This value is small compared with the Heisenberg exchange interactions $\tilde{J}_0 \sim 14.6 \text{ meV}$ and thus plays a negligible role in the physics we address. The dependence of interlayer exchange on \mathcal{E} from DFT calculations is negligible for practical electric field strengths. Combining the DFT result for λ with either the Monte-Carlo or the mean-field theory results illustrated in Fig. 2 yields values for the ratio of the net magnetization per volume to the electric field $\sim 1 \times 10^{-3}$ ¹ which is dimensionless in cgs units and is one order larger than the corresponding values of 10^{-4} in classic magnetoelectric materials like chromia,⁶⁵⁻⁶⁷ slightly smaller than that of topological magnetoelectric coefficient (which is around 3×10^{-3}).

Influence of Electrostatic Doping CrI_3

The possibility of electrostatic doping expands the phenomenology of magnetoelectric response beyond the effects of an interlayer potential difference introduced by perpendicular

¹As ref.²¹ pointed out, off-diagonal magneto-electric response coefficients are allowed by symmetry for some stacking arrangements. Based on our DFT calculations, it seems that the off-diagonal response is weak. We place an upper bound as $\sim 5 \times 10^{-5}$ on the off-diagonal response in both R3 and C2m bilayer cases.

electric fields. Consideration of carrier doping is experimentally relevant since typical samples are often accidentally doped; typical carrier densities have been reported to range from $4.4 \times 10^{12} \text{cm}^{-2}$ ¹⁸ to $2.3 \times 10^{13} \text{cm}^{-2}$.¹⁷ Both carrier density and electric fields can be controlled independently in dual gated bilayers.

At finite but low carrier densities, the $T = 0$ energies of the FM and AF states at a given average electric field are given by:

$$\begin{aligned} E_{\text{FM}} &= E_0^{\text{FM}} - \theta(-n)E_c^{\text{F}}nA + \theta(n)E_v^{\text{F}}nA \\ E_{\text{AF}} &= E_0^{\text{AF}} - \theta(-n)E_c^{\text{AF}}nA + \theta(n)E_v^{\text{AF}}nA \end{aligned} \quad (8)$$

where $E_0^{\text{FM/AF}}$ is the energy per 2D unit cell in the absence of carriers, n is the carrier density per unit cell defined as negative for electrons and positive for holes defining the value of the Heavyside step function $\theta(n)$, A is the unit cell area $\sqrt{3}a^2/2$ where $a = 6.863$ angstrom is the lattice constant, and $E_{c/v}$ are the conduction/valence band edge energies.

Doping generally favors ferromagnetic states because the ferromagnetic state has a smaller bandgap, allowing carriers to be introduced with a smaller band energy cost. As show in Fig. 3(b), we estimate that carrier densities of around $1.5 \times 10^{12} \text{cm}^{-2}$ for electrons and $3 \times 10^{12} \text{cm}^{-2}$ for holes are sufficient to induce transitions from antiferromagnetic to ferromagnetic state. We expect that variations in the total carrier density with gates can change the magnitude of the interlayer coupling J_v . Increasing J_v results in magneto-electric effects that are weaker at their peak, but sizable over a broader range of temperatures.

Conclusions

We have shown that antiferromagnetic van der Waals bilayers have a sizable magneto-electric response to gate-applied displacement fields because of their weak interlayer exchange interactions. The size of the response has a stronger peak, but a lower one away from the critical temperature. The sign of this response depends on which of the two layers has a

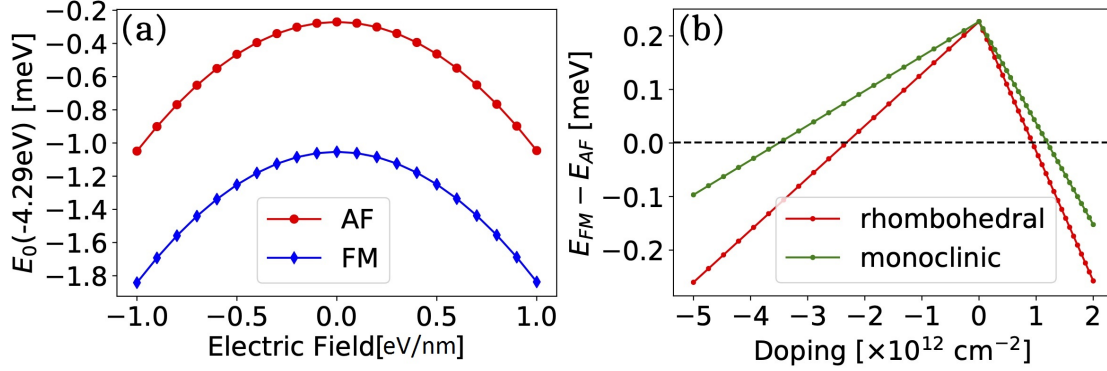


Figure 3: Magnetoelectric Effect: (a) Dependence of ground-state energy on electric field obtained from DFT calculations for the rhombohedrally stacked bilayer. At zero-carrier density, the ground state energy has a quadratic dependence on the electric field. (b) Difference between ground state energies as a function of carrier density given in units of electrons per cm^{-2} calculated from Eq. (8) defined as negative (positive) for electron (hole) doping.

particular spin orientation, allowing information encoded in the antiferromagnetic bilayer’s magnetic configuration to be read electrically by measuring the Hall conductivity of the bilayer. Inducing net magnetism electrically allows, the antiferromagnetic configuration to be rewritten by external magnetic fields. In dual gated geometries, in which carrier density and displacement field can be varied independently, the size and temperature dependence of the magneto-electric response can be varied *in situ* by varying the strength of interlayer interactions. These properties add to the motivation for the development of antiferromagnetic bilayers with robust room temperature order.

Acknowledgement

C. L. and A. H. M. were supported by the SHINES Center, funded by the U.S. Department of Energy, Office of Science, Basic Energy Sciences under Award DE-SC0012670, and the Welch Foundation under grant TBF1473. B. L. C. was supported by the Basic Science Research Program through the National Research Foundation of Korea (NRF) funded by the Ministry of Education (No. 2018R1A6A1A06024977) and grant NRF-2020R1A5A1016518.

N. B was supported by the grant NRF-2020R1A2C3009142 and J. J. by Samsung Science and Technology Foundation under Project No. SSTF-BA1802-06. K. N. was supported by the JSPS KAKENHI (Grant No. JP15H05854, JP15K21717, JP17K05485) and JST CREST (JPMJCR18T2). We acknowledge computer time allocations from the Texas Advanced Computing Center and from KISTI through grant KSC-2020-CRE-0072.

Supporting Information Available

This material is available free of charge via the internet at <http://pubs.acs.org>.

- Details of crystal structure, DFT calculations, strain effect, reliability of interlayer exchange coupling, Monte Carlo simulation, and mean-field theory.

References

- (1) Wang, W.-G.; Li, M.; Hageman, S.; Chien, C. L. Electric-field-assisted switching in magnetic tunnel junctions. *Nat. Mater.* **2011**, *11*, 64.
- (2) Maruyama, T.; Shiota, Y.; Nozaki, T.; Ohta, K.; Toda, N.; Mizuguchi, M.; Tulapurkar, A. A.; Shinjo, T.; Shiraishi, M.; Mizukami, S.; Ando, Y.; Suzuki, Y. Large voltage-induced magnetic anisotropy change in a few atomic layers of iron. *Nat. Nanotechnol.* **2009**, *4*, 158.
- (3) Wu, S. M.; Cybart, S. A.; Yu, P.; Rossell, M. D.; Zhang, J. X.; Ramesh, R.; Dynes, R. C. Reversible electric control of exchange bias in a multiferroic field-effect device. *Nat. Mater.* **2010**, *9*, 756.
- (4) He, X.; Wang, Y.; Wu, N.; Caruso, A. N.; Vescovo, E.; Belashchenko, K. D.; Dowben, P. A.; Binek, C. Robust isothermal electric control of exchange bias at room temperature. *Nat. Mater.* **2010**, *9*, 579.

- (5) Žutić, I.; Fabian, J.; Das Sarma, S. Spintronics: Fundamentals and applications. *Rev. Mod. Phys.* **2004**, *76*, 323–410.
- (6) Matsukura, F.; Tokura, Y.; Ohno, H. Control of magnetism by electric fields. *Nat. Nanotechnol.* **2015**, *10*, 209.
- (7) Jungwirth, T.; Sinova, J.; Manchon, A.; Marti, X.; Wunderlich, J.; Felser, C. The multiple directions of antiferromagnetic spintronics. *Nature Physics* **2018**, *14*, 200–203.
- (8) Baltz, V.; Manchon, A.; Tsoi, M.; Moriyama, T.; Ono, T.; Tserkovnyak, Y. Antiferromagnetic spintronics. *Rev. Mod. Phys.* **2018**, *90*, 015005.
- (9) Jungwirth, T.; Marti, X.; Wadley, P.; Wunderlich, J. Antiferromagnetic spintronics. *Nature nanotechnology* **2016**, *11*, 231.
- (10) Huang, B.; Clark, G.; Navarro-Moratalla, E.; Klein, D. R.; Cheng, R.; Seyler, K. L.; Zhong, D.; Schmidgall, E.; McGuire, M. A.; Cobden, D. H. Layer-dependent ferromagnetism in a van der Waals crystal down to the monolayer limit. *Nature* **2017**, *546*, 270.
- (11) Gong, C.; Li, L.; Li, Z.; Ji, H.; Stern, A.; Xia, Y.; Cao, T.; Bao, W.; Wang, C.; Wang, Y.; Qiu, Z. Q.; Cava, R. J.; Louie, S. G.; Xia, J.; Zhang, X. Discovery of intrinsic ferromagnetism in two-dimensional van der Waals crystals. *Nature* **2017**, *546*, 265.
- (12) Song, T.; Cai, X.; Tu, M. W.-Y.; Zhang, X.; Huang, B.; Wilson, N. P.; Seyler, K. L.; Zhu, L.; Taniguchi, T.; Watanabe, K., et al. Giant tunneling magnetoresistance in spin-filter van der Waals heterostructures. *Science* **2018**, *360*, 1214–1218.
- (13) Wang, Z.; Gutiérrez-Lezama, I.; Ubrig, N.; Kroner, M.; Gibertini, M.; Taniguchi, T.; Watanabe, K.; Imamoğlu, A.; Giannini, E.; Morpurgo, A. F. Very large tunneling magnetoresistance in layered magnetic semiconductor CrI₃. *Nat. Comm.* **2018**, *9*, 2516.

- (14) Kim, H. H.; Yang, B.; Patel, T.; Sfigakis, F.; Li, C.; Tian, S.; Lei, H.; Tsen, A. W. One million percent tunnel magnetoresistance in a magnetic van der Waals heterostructure. *Nano Lett.* **2018**, *18*, 4885–4890.
- (15) Klein, D. R.; MacNeill, D.; Lado, J. L.; Soriano, D.; Navarro-Moratalla, E.; Watanabe, K.; Taniguchi, T.; Manni, S.; Canfield, P.; Fernández-Rossier, J.; et al., Probing magnetism in 2D van der Waals crystalline insulators via electron tunneling. *Science* **2018**, *360*, 1218–1222.
- (16) Jiang, S.; Shan, J.; Mak, K. F. Electric-field switching of two-dimensional van der Waals magnets. *Nature Materials* **2018**, *17*, 406–410.
- (17) Jiang, S.; Li, L.; Wang, Z.; Mak, K. F.; Shan, J. Controlling magnetism in 2D CrI₃ by electrostatic doping. *Nature Nanotechnology* **2018**, *13*, 549–553.
- (18) Huang, B.; Clark, G.; Klein, D. R.; MacNeill, D.; Navarro-Moratalla, E.; Seyler, K. L.; Wilson, N.; McGuire, M. A.; Cobden, D. H.; Xiao, D.; et al., Electrical control of 2D magnetism in bilayer CrI₃. *Nature Nanotechnology* **2018**, *13*, 544–548.
- (19) Li, T.; Jiang, S.; Sivadas, N.; Wang, Z.; Xu, Y.; Weber, D.; Goldberger, J. E.; Watanabe, K.; Taniguchi, T.; Fennie, C. J.; et al., Pressure-controlled interlayer magnetism in atomically thin CrI₃. *Nature Materials* **2019**, *18*, 1303–1308.
- (20) Soriano, D.; Cardoso, C.; Fernández-Rossier, J. Interplay between interlayer exchange and stacking in CrI₃ bilayers. *Solid State Communications* **2019**, *299*, 113662.
- (21) Sivadas, N.; Okamoto, S.; Xu, X.; Fennie, C. J.; Xiao, D. Stacking-dependent magnetism in bilayer CrI₃. *Nano Lett.* **2018**, *18*, 7658–7664.
- (22) Jiang, P.; Wang, C.; Chen, D.; Zhong, Z.; Yuan, Z.; Lu, Z.-Y.; Ji, W. Stacking tunable interlayer magnetism in bilayer CrI₃. *Phys. Rev. B* **2019**, *99*, 144401.

- (23) Jang, S. W.; Jeong, M. Y.; Yoon, H.; Ryee, S.; Han, M. J. Microscopic understanding of magnetic interactions in bilayer CrI₃. *Phys. Rev. Materials* **2019**, *3*, 031001.
- (24) Chen, W.; Sun, Z.; Wang, Z.; Gu, L.; Xu, X.; Wu, S.; Gao, C. Direct observation of van der Waals stacking-dependent interlayer magnetism. *Science* **2019**, *366*, 983–987.
- (25) Guo, K.; Deng, B.; Liu, Z.; Gao, C.; Shi, Z.; Bi, L.; Zhang, L.; Lu, H.; Zhou, P.; Zhang, L.; et al., Layer dependence of stacking order in nonencapsulated few-layer CrI₃. *Science China Materials* **2019**, *63*, 413–420.
- (26) Soriano, D.; Katsnelson, M. I.; Fernández-Rossier, J. Magnetic Two-Dimensional Chromium Trihalides: A Theoretical Perspective. *Nano Letters* **2020**, *20*, 6225–6234.
- (27) Thiel, L.; Wang, Z.; Tschudin, M. A.; Rohner, D.; Gutiérrez-Lezama, I.; Ubrig, N.; Gibertini, M.; Giannini, E.; Morpurgo, A. F.; Maletinsky, P. Probing magnetism in 2D materials at the nanoscale with single-spin microscopy. *Science* **2019**, *364*, 973–976.
- (28) Sun, Z.; Yi, Y.; Song, T.; Clark, G.; Huang, B.; Shan, Y.; Wu, S.; Huang, D.; Gao, C.; Chen, Z.; et al., Giant nonreciprocal second-harmonic generation from antiferromagnetic bilayer CrI₃. *Nature* **2019**, *572*, 497–501.
- (29) Zhang, Y.; Wu, X.; Lyu, B.; Wu, M.; Zhao, S.; Chen, J.; Jia, M.; Zhang, C.; Wang, L.; Wang, X., et al. Magnetic Order-Induced Polarization Anomaly of Raman Scattering in 2D Magnet CrI₃. *Nano Letters* **2019**, *20*, 729–734.
- (30) McCreary, A.; Mai, T. T.; Utermohlen, F. G.; Simpson, J. R.; Garrity, K. F.; Feng, X.; Shcherbakov, D.; Zhu, Y.; Hu, J.; Weber, D.; et al., Distinct magneto-Raman signatures of spin-flip phase transitions in CrI₃. *Nature Communications* **2020**, *11*.
- (31) Ubrig, N.; Wang, Z.; Teyssier, J.; Taniguchi, T.; Watanabe, K.; Giannini, E.; Morpurgo, A. F.; Gibertini, M. Low-temperature monoclinic layer stacking in atomically thin CrI₃ crystals. *2D Materials* **2019**, *7*, 015007.

- (32) Klein, D. R.; MacNeill, D.; Song, Q.; Larson, D. T.; Fang, S.; Xu, M.; Ribeiro, R. A.; Canfield, P. C.; Kaxiras, E.; Comin, R.; et al., Enhancement of interlayer exchange in an ultrathin two-dimensional magnet. *Nature Physics* **2019**, *15*, 1255–1260.
- (33) Pershoguba, S. S.; Banerjee, S.; Lashley, J. C.; Park, J.; Ågren, H.; Aeppli, G.; Balatsky, A. V. Dirac Magnons in Honeycomb Ferromagnets. *Phys. Rev. X* **2018**, *8*, 011010.
- (34) Chisnell, R.; Helton, J. S.; Freedman, D. E.; Singh, D. K.; Bewley, R. I.; Nocera, D. G.; Lee, Y. S. Topological Magnon Bands in a Kagome Lattice Ferromagnet. *Phys. Rev. Lett.* **2015**, *115*, 147201.
- (35) Owerre, S. Topological magnon bands and unconventional thermal Hall effect on the frustrated honeycomb and bilayer triangular lattice. *Journal of Physics: Condensed Matter* **2017**, *29*, 385801.
- (36) Liu, J.; Shi, M.; Lu, J.; Anantram, M. P. Analysis of electrical-field-dependent Dzyaloshinskii-Moriya interaction and magnetocrystalline anisotropy in a two-dimensional ferromagnetic monolayer. *Phys. Rev. B* **2018**, *97*, 054416.
- (37) Bonilla, M.; Kolekar, S.; Ma, Y.; Diaz, H. C.; Kalappattil, V.; Das, R.; Eggers, T.; Gutierrez, H. R.; Phan, M.-H.; Batzill, M. Strong room-temperature ferromagnetism in VSe₂ monolayers on van der Waals substrates. *Nat. Nanotechnol.* **2018**, *13*, 289–293.
- (38) OHara, D. J.; Zhu, T.; Trout, A. H.; Ahmed, A. S.; Luo, Y. K.; Lee, C. H.; Brenner, M. R.; Rajan, S.; Gupta, J. A.; McComb, D. W.; Kawakami, R. K. Room Temperature Intrinsic Ferromagnetism in Epitaxial Manganese Selenide Films in the Monolayer Limit. *Nano Lett.* **2018**, *18*, 3125–3131.
- (39) Yun, S. J.; Duong, D. L.; Ha, D. M.; Singh, K.; Phan, T. L.; Choi, W.; Kim, Y.; Lee, Y. H. Ferromagnetic Order at Room Temperature in Monolayer WSe₂ Semiconductor via Vanadium Dopant. *Advanced Science* **2020**, *7*, 1903076.

- (40) Sun, X. et al. Room temperature 2D ferromagnetism in few-layered 1T-CrTe₂. *Nano Research* **2020**, *13*, 3358–3363.
- (41) Lado, J. L.; Fernández-Rossier, J. On the origin of magnetic anisotropy in two dimensional CrI₃. *2D Materials* **2017**, *4*, 035002.
- (42) Lee, I.; Utermohlen, F. G.; Weber, D.; Hwang, K.; Zhang, C.; van Tol, J.; Goldberger, J. E.; Trivedi, N.; Hammel, P. C. Fundamental Spin Interactions Underlying the Magnetic Anisotropy in the Kitaev Ferromagnet CrI₃. *Phys. Rev. Lett.* **2020**, *124*, 017201.
- (43) Chen, L. et al. Magnetic anisotropy in ferromagnetic CrI₃. *Phys. Rev. B* **2020**, *101*, 134418.
- (44) Olsen, T. Theory and simulations of critical temperatures in CrI₃ and other 2D materials: easy-axis magnetic order and easy-plane Kosterlitz–Thouless transitions. *MRS Communications* **2019**, *9*, 1142–1150.
- (45) Xu, C.; Feng, J.; Xiang, H.; Bellaiche, L. Interplay between Kitaev interaction and single ion anisotropy in ferromagnetic CrI₃ and CrGeTe₃ monolayers. *npj Computational Materials* **2018**, *4*, 1–6.
- (46) Kim, J.; Kim, K.-W.; Kim, B.; Kang, C.-J.; Shin, D.; Lee, S.-H.; Min, B.-C.; Park, N. Exploitable magnetic anisotropy of the two-dimensional magnet CrI₃. *Nano Letters* **2019**, *20*, 929–935.
- (47) Webster, L.; Yan, J.-A. Strain-tunable magnetic anisotropy in monolayer CrCl₃, CrBr₃, and CrI₃. *Phys. Rev. B* **2018**, *98*, 144411.
- (48) Besbes, O.; Nikolaev, S.; Meskini, N.; Solovyev, I. Microscopic origin of ferromagnetism in the trihalides CrCl₃ and CrI₃. *Phys. Rev. B* **2019**, *99*, 104432.

- (49) Pizzochero, M.; Yadav, R.; Yazyev, O. V. Magnetic exchange interactions in monolayer CrI₃ from many-body wavefunction calculations. *2D Materials* **2020**, *7*, 035005.
- (50) Richter, N.; Weber, D.; Martin, F.; Singh, N.; Schwingenschlögl, U.; Lotsch, B. V.; Kläui, M. Temperature-dependent magnetic anisotropy in the layered magnetic semiconductors CrI₃ and CrBr₃. *Phys. Rev. Materials* **2018**, *2*, 024004.
- (51) Torelli, D.; Olsen, T. Calculating critical temperatures for ferromagnetic order in two-dimensional materials. *2D Materials* **2018**, *6*, 015028.
- (52) Kresse, G.; Hafner, J. Ab initio molecular dynamics for liquid metals. *Phys. Rev. B* **1993**, *47*, 558–561.
- (53) Giannozzi, P. et al. QUANTUM ESPRESSO: a modular and open-source software project for quantum simulations of materials. *J. Phys.: Condens. Matter* **2009**, *21*, 395502.
- (54) J. P. Perdew, K. B.; Ernzerhof, M. Generalized Gradient Approximation Made Simple. *Phys. Rev. Lett.* **1997**, *77*, 3865.
- (55) Grimme, S. Semiempirical GGA-type density functional constructed with a long-range dispersion correction. *J. Comput. Chem.* **2006**, *27*, 1787.
- (56) Bucko, T.; Hafner, J.; Lebegue, S.; Angyán, J. G. Improved description of the structure of molecular and layered crystals: ab initio DFT calculations with van der Waals corrections. *The Journal of Physical Chemistry A* **2010**, *114*, 11814–11824.
- (57) Neugebauer, J.; Scheffler, M. Adsorbate-substrate and adsorbate-adsorbate interactions of Na and K adlayers on Al(111). *Phys. Rev. B* **1992**, *46*, 16067–16080.
- (58) Makov, G.; Payne, M. C. Periodic boundary conditions in ab initio calculations. *Phys. Rev. B* **1995**, *51*, 4014–4022.

- (59) See Supporting Information for details of crystal structure, DFT calculations, strain effect and reliability interlayer exchange coupling, Monte Carlo simulation, and mean-field theory.
- (60) Zhang, W.-B.; Qu, Q.; Zhu, P.; Lam, C.-H. Robust intrinsic ferromagnetism and half semiconductivity in stable two-dimensional single-layer chromium trihalides. *J. Mater. Chem. C* **2015**, *3*, 12457–12468.
- (61) McGuire, M. A.; Dixit, H.; Cooper, V. R.; Sales, B. C. Coupling of Crystal Structure and Magnetism in the Layered, Ferromagnetic Insulator CrI₃. *Chem. Mater.* **2015**, *27*, 612–620.
- (62) Ding, Y.; Wang, Y.; Ni, J.; Shi, L.; Shi, S.; Tang, W. First principles study of structural, vibrational and electronic properties of graphene-like MX₂ (M=Mo, Nb, W, Ta; X=S, Se, Te) monolayers. *Physica B* **2011**, *406*, 2254–2260.
- (63) Wang, H.; Eyert, V.; U., S. Electronic structure and magnetic ordering of the semiconducting chromium trihalides CrCl₃, CrBr₃, and CrI₃. *J. Phys. Condens. Matter.* **2011**, *23*, 116003.
- (64) Feldkemper, S.; Weber, W. Generalized calculation of magnetic coupling constants for Mott-Hubbard insulators: Application to ferromagnetic Cr compounds. *Phys. Rev. B* **1998**, *57*, 7755–7766.
- (65) Wang, J.; Lei, C.; Macdonald, A. H.; Binek, C. Dynamic axion field in the magnetoelectric antiferromagnet chromia. **2019**, *arXiv e-prints*, <https://arxiv.org/abs/1901.08536> (accessed on 12.02.2021).
- (66) Astrov, D. Magnetoelectric effect in chromium oxide. *Sov. Phys. JETP* **1961**, *13*, 729–733.

- (67) Mostovoy, M.; Scaramucci, A.; Spaldin, N. A.; Delaney, K. T. Temperature-Dependent Magnetoelectric Effect from First Principles. *Phys. Rev. Lett.* **2010**, *105*, 087202.